



Structural characterization and Hirshfeld surface analysis of a Co^{II} complex with imidazo[1,2-*a*]-pyridine

Saikat Kumar Seth*

Department of Physics, Jadavpur University, Kolkata 700 032, India. *Correspondence e-mail: skseth@phys.jdvvu.ac.in

Received 14 November 2017

Accepted 5 March 2018

Edited by C. Massera, Università di Parma, Italy

Keywords: crystal structure; Co^{II} complex with imidazopyridine; noncovalent interactions; supramolecular assembly; Hirshfeld surface; fingerprint plot.

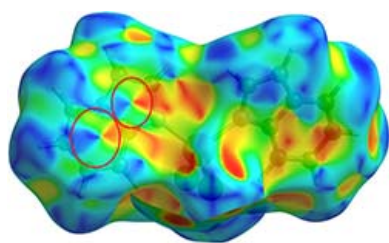
Supporting information: this article has supporting information at journals.iucr.org/e

A new mononuclear tetrahedral Co^{II} complex, dichloridobis(imidazo[1,2-*a*]-pyridine-*κ*N¹)cobalt(II), [CoCl₂(C₇H₆N₂)₂], has been synthesized using a bioactive imidazopyridine ligand. X-ray crystallography reveals that the solid-state structure of the title complex exhibits both C—H···Cl and π – π stacking interactions in building supramolecular assemblies. Indeed, the molecules are linked by C—H···Cl interactions into a two-dimensional framework, with finite zero-dimensional dimeric units as building blocks, whereas π – π stacking plays a crucial role in building a supramolecular layered network. An exhaustive investigation of the diverse intermolecular interactions *via* Hirshfeld surface analysis enables contributions to the crystal packing of the title complex to be quantified. The fingerprint plots associated with the Hirshfeld surface clearly display each significant interaction involved in the structure, by quantifying them in an effective visual manner.

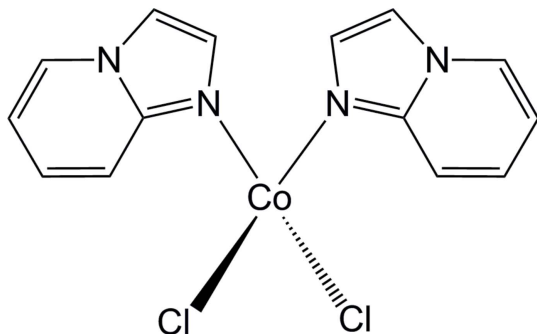
1. Chemical context

In the realm of the synthesis of heterocyclic compounds, imidazopyridines have proven to be a most important class of molecules and have attracted significant interest because of their promising applications. They are biologically important and have shown a wide variety of pharmacological effects (Adib *et al.*, 2011): anti-inflammatory (Rupert *et al.*, 2003), antiviral (Puerstinger *et al.*, 2007), antiulcer (Kaminski & Doweyko, 1997), antibacterial (Rival *et al.*, 1992), antifungal (Rival *et al.*, 1991), antiprotozoal (Biftu *et al.*, 2006; Ismail *et al.*, 2008), antiherpes (Gudmundsson & Johns, 2007; Véron *et al.*, 2007), and for the treatment of hepatitis C (Bravi *et al.*, 2007), and HIV (Gudmundsson & Boggs, 2007). These medically relevant compounds exhibit a wide range of activities including anti-herpes, antiapoptotic, sedative, anxiolytic, anticonvulsant, muscle relaxant, analgesic, antituberculosis and anticancer actions (Dymińska, 2015; Bagdi *et al.*, 2015). The core structure of imidazo[1,2-*a*]pyridine is present in several drugs, such as zolpidem, alpidem, zolimidine, olprione, GSK812397, saripidem, and necopidem (Gunja, 2013; Harrison & Keating, 2005; Bagdi *et al.*, 2015). Besides, this heterocyclic scaffold has attracted tremendous attention from the synthetic community due to its prevalence in dyes, ligands for metal catalysts, and electronic materials (Enguehard-Gueiffier & Gueiffier, 2007; Prostota *et al.*, 2013; Ke *et al.*, 2013).

Inspired by the manifold potential applications of imidazo[1,2-*a*]pyridine, we focused our attention on its



coordination behavior towards metal ions and to the structural features of the resulting complexes. Herein, the crystal and molecular structure of a new Co^{II} complex with imidazo-[1,2-*a*]pyridine is described, along with an investigation of the intermolecular interactions *via* Hirshfeld surface analysis.



2. Structural commentary

The molecular structure of the title complex is shown in Fig. 1. The Co^{II} ion is located on a twofold axis, so that half of the complex is generated by symmetry. The metal center is coordinated to the nitrogen atoms of two imidazopyridine ligands and to two chlorine ions, and shows a tetrahedral geometry with angles ranging from 107.70 (5) to 112.44 (5)°. Selected geometric parameters around Co^{II} are reported in Table 1. The imidazopyridine moiety is planar, with a dihedral angle between the rings of 2.47 (3)°. In the imidazopyridine moiety, atoms C6 and C4 show the largest deviations in opposite directions [C6: +0.034 (1) and N1: -0.037 (1)] from the least-squares mean plane through the atoms N1/C6/C7/N2/C1–C5.

3. Supramolecular features

The title structure exhibits intermolecular $\text{C}-\text{H}\cdots\text{Cl}$ and $\pi-\pi$ stacking interactions; the details are included in Tables 2 and 3, respectively. It is convenient to consider the ‘substructures’ generated by each interaction individually, and then combine these substructures to build up the supramolecular assembly.

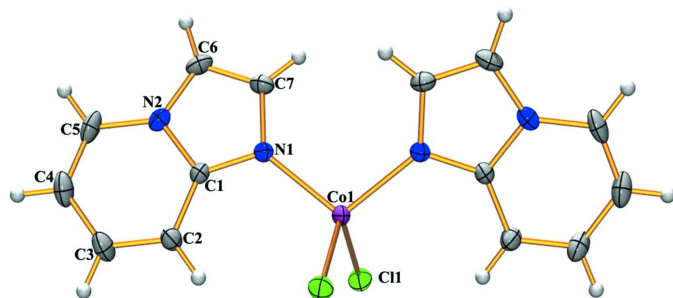


Figure 1
ORTEP view with atom-numbering scheme of the title complex with displacement ellipsoids drawn at the 30% probability level. The unlabeled counterpart is generated by the symmetry operation $-x + \frac{1}{2}, y, -z + \frac{3}{2}$.

Table 1
Selected geometric parameters (Å, °).

Co1–N1	2.0168 (4)	Co1–Cl1	2.2556 (5)
N1–Co1–N1 ⁱ	107.70 (5)	N1 ⁱ –Co1–Cl1	112.44 (5)
N1–Co1–Cl1	106.83 (1)	Cl1–Co1–Cl1 ⁱ	110.64 (4)

Symmetry code: (i) $-x + \frac{1}{2}, y, -z + \frac{3}{2}$.

Table 2
Hydrogen-bond geometry (Å, °).

<i>D</i> –H \cdots <i>A</i>	<i>D</i> –H	H \cdots <i>A</i>	<i>D</i> \cdots <i>A</i>	<i>D</i> –H \cdots <i>A</i>
C5–H5 \cdots Cl1 ⁱⁱ	0.93	2.89	3.663 (1)	141
C7–H7 \cdots Cl1 ⁱⁱⁱ	0.93	2.88	3.734 (1)	153

Symmetry codes: (ii) $-x, -y, -z + 1$; (iii) $x, y - 1, z$.

The first substructure is formed considering the pyridine ring carbon atom C5 in a general position, which acts as donor to the Cl1 atom at $(-x, -y, 1 - z)$. This C5–H5 \cdots Cl1 interaction and its centrosymmetric analogue generate an $R_2^2(18)$ dimeric ring (*M*) centered at $(0, 0, 1/2)$ (Fig. 2). A second substructure is formed *via* pairs of symmetry-related C7–H7 \cdots Cl1($x, -1 + y, z$) interactions, which generate a dimeric $R_2^2(10)$ ring (*N*) (Fig. 2). The propagation of these dimers produces two infinite chains, the first running parallel to the $(\bar{1}01)$ plane and the second running parallel to the $[010]$ direction. The interconnection of the two chains leads to the generation of another tetrameric $R_4^2(14)$ ring motif (*P*). Thus, the two types of $R_2^2(18)$ and $R_4^2(14)$ rings are alternately linked into infinite *MPMP*... chains along the $[010]$ direction

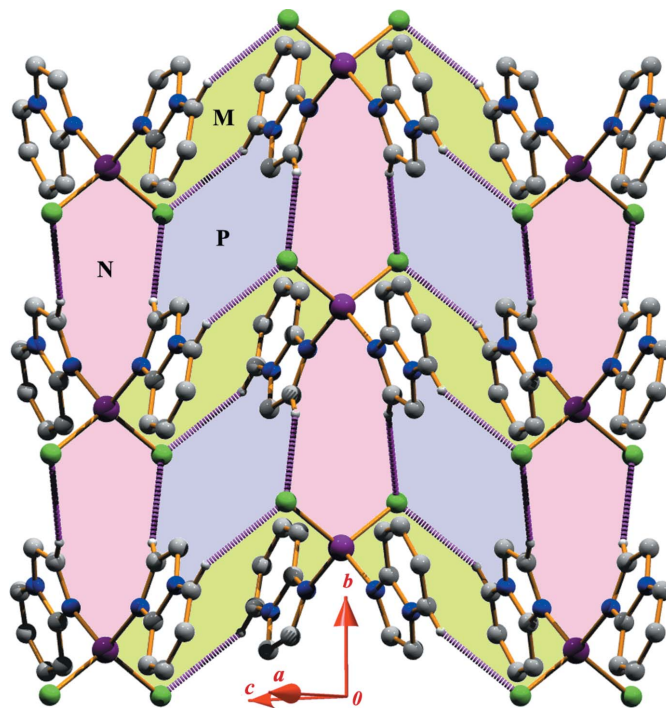


Figure 2
Formation of a two-dimensional supramolecular network generated through self-complementary $\text{C}-\text{H}\cdots\text{Cl}$ interactions.

Table 3

Geometrical parameters (Å, °) for π - π stacking.

(a) $Cg1$ and $Cg2$ are the centroids of the (N1/C1/N2/C6/C7) and (N2/C1–C5) rings, respectively; (b) centroid–centroid distance between ring i and ring j ; (c) vertical distance from ring centroid i to ring j ; (d) vertical distance from ring centroid j to ring i ; (e) dihedral angle between the first ring mean plane and the second ring mean plane of the partner molecule; (f) angle between the centroid of the first ring and the second ring; (g) angle between the centroid of the first ring and the normal to the mean plane of the second ring of the partner molecule.

Rings i – j^a	Rc^b	$R1v^c$	$R2v^d$	α^e	β^f	γ^g	Slippage
$Cg1 \cdots Cg1^{ii}$	3.6414 (16)	–3.4980 (8)	–3.4980 (8)	0.0	16.13	16.13	1.012
$Cg1 \cdots Cg2^{ii}$	3.9583 (16)	–3.5303 (9)	–3.5035 (9)	2.47	27.73	26.89	–
$Cg1 \cdots Cg2^{iv}$	3.8371 (16)	3.4625 (9)	3.4846 (9)	2.47	24.75	25.53	–
$Cg2 \cdots Cg2^{iv}$	3.5293 (16)	3.4671 (9)	3.4671 (9)	0.0	10.77	10.77	0.659

Symmetry codes: (ii) $-x, -y, -z + 1$; (iv) $-x + 1, -y, -z + 1$.

whereas the $R_2^2(10)$ and $R_4^2(14)$ rings are linked alternately into an infinite $NPNP \dots$ chain parallel to the ($\bar{1}01$) plane (Fig. 2).

Another substructure can be described considering that the molecules, because of their self-complementarity nature, are juxtaposed through π - π stacking interactions (Seth *et al.*, 2011a, 2013; Manna *et al.*, 2013, 2014a). The molecular packing of the complex is such that the π - π stacking interactions between the pyridine rings, as well as between the imidazo rings, are optimized. The pyridine rings of the molecules at (x, y, z) and $(-x + 1, -y, -z + 1)$ are strictly parallel, with an interplanar spacing of 3.4671 (9) Å and a ring-centroid separation of 3.5293 (16) Å, corresponding to a ring offset of 0.659 Å. In addition, the imidazo rings at (x, y, z) and $(-x, -y, -z + 1)$ are juxtaposed through face-to-face π -stacking with an inter-centroid separation of 3.6414 (16) Å. Moreover, the imidazo and pyridine rings of the parent molecules are also involved into multi π -stacking interactions with each other. In particular, the interplanar spacing between the imidazo ring in a general position and the pyridine rings at $(-x, -y, -z + 1)$ and $(-x + 1, -y, -z + 1)$ are of 3.5303 (9) and 3.4625 (9) Å, respectively, while the relative ring-centroid separations are 3.9583 (16) and 3.8371 (16) Å. These π - π stacking interactions result in a two-dimensional supramolecular layered assembly parallel to the (010) plane (Fig. 3).

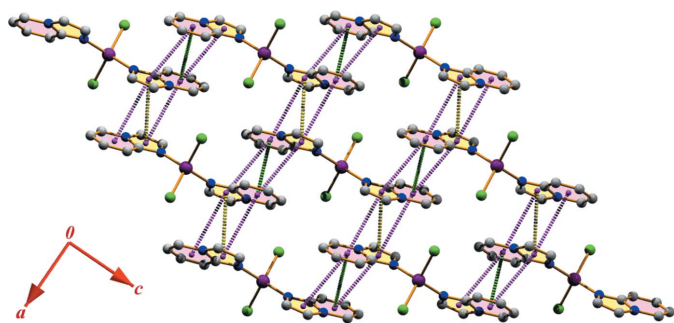


Figure 3

Monomeric units linked through multi π - π stacking interactions leading to the formation of a supramolecular layered assembly. Color codes: the green and yellow dotted lines denote π - π stacking interactions between two pyridine rings and two imidazo rings, respectively, whereas π - π stacking interactions between pyridine and imidazo rings are represented by pink dotted lines.

4. Hirshfeld surface analysis

Molecular Hirshfeld surfaces (Spackman & McKinnon, 2002) in the crystal structure are constructed considering the electron distribution calculated as the sum of spherical atom electron densities (Spackman & Byrom, 1997; McKinnon *et al.*, 1998). The normalized contact distance (d_{norm}) based on both d_e and d_i , and the van der Waals (vdw) radii of the atom, given by the equation

$$d_{\text{norm}} = \frac{d_i - r_i^{\text{vdw}}}{r_i^{\text{vdw}}} + \frac{d_e - r_e^{\text{vdw}}}{r_e^{\text{vdw}}}$$

enable the identification of the regions of particular importance to intermolecular interactions (McKinnon *et al.*, 2007). The combination of d_e and d_i in the form of a two-dimensional fingerprint plot (Rohl *et al.*, 2008) provides a summary of the intermolecular contacts in the crystal (Spackman & McKinnon, 2002). The Hirshfeld surfaces are mapped with d_{norm} , and the two-dimensional fingerprint plots presented in this work were generated using *CrystalExplorer 3.1* (Wolff *et al.*, 2012).

The pattern of the intermolecular interactions of the solid-state structure of the title complex prompted us to explore and quantify the contribution of the non-covalent interactions in the crystal packing, as well as the importance of the C–H \cdots Cl bonding in directing the organization of the extended supramolecular network (Seth *et al.*, 2011a,b, Manna *et al.*,

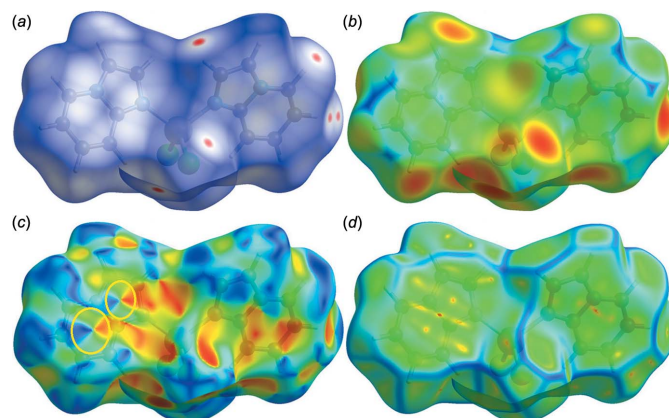


Figure 4

Hirshfeld surfaces of the title complex mapped with (a) d_{norm} , (b) d_e , (c) shape-index and (d) curvedness.

2012; Seth, 2013; Mitra *et al.*, 2014). In this present investigation, the contacts responsible for building the supramolecular assembly were evaluated with respect to their contribution to the overall stability of the crystal structure. In this context, the Hirshfeld surface analysis (Spackman & McKinnon, 2002; Seth *et al.*, 2011a,b,c,d; Mitra *et al.*, 2013) of the title complex was performed and the results are illustrated in Fig. 4. The surfaces represented were mapped over d_{norm} , d_e , shape-index and curvedness in the ranges -0.0620 to 0.9660 Å, 1.0626 to 2.4714 Å, -1.0000 to 1.0000 Å and -4.0000 to 0.4000 Å, respectively. The information regarding the intermolecular interactions summarized in Tables 2 and 3 are visible as spots on the Hirshfeld surfaces (Fig. 4). For instance, the distinct circular depressions (red spots) on the d_{norm} surface (Fig. 4a) are due to the C—H...Cl contacts, whereas other visible spots are due to H...H contacts. From the Hirshfeld surfaces, it is also evident that the molecules are related to one another by π - π stacking interactions, as can be inferred from inspection of the adjacent red and blue triangles (highlighted by yellow circles) on the shape-index surface (Fig. 4c). Indeed, the pattern of red and blue triangles in the same region of the shape-index surface is characteristic of π - π stacking interactions; the blue triangles represent convex regions resulting from the presence of ring carbon atoms of the molecule inside the surface, while the red triangles represent concave regions

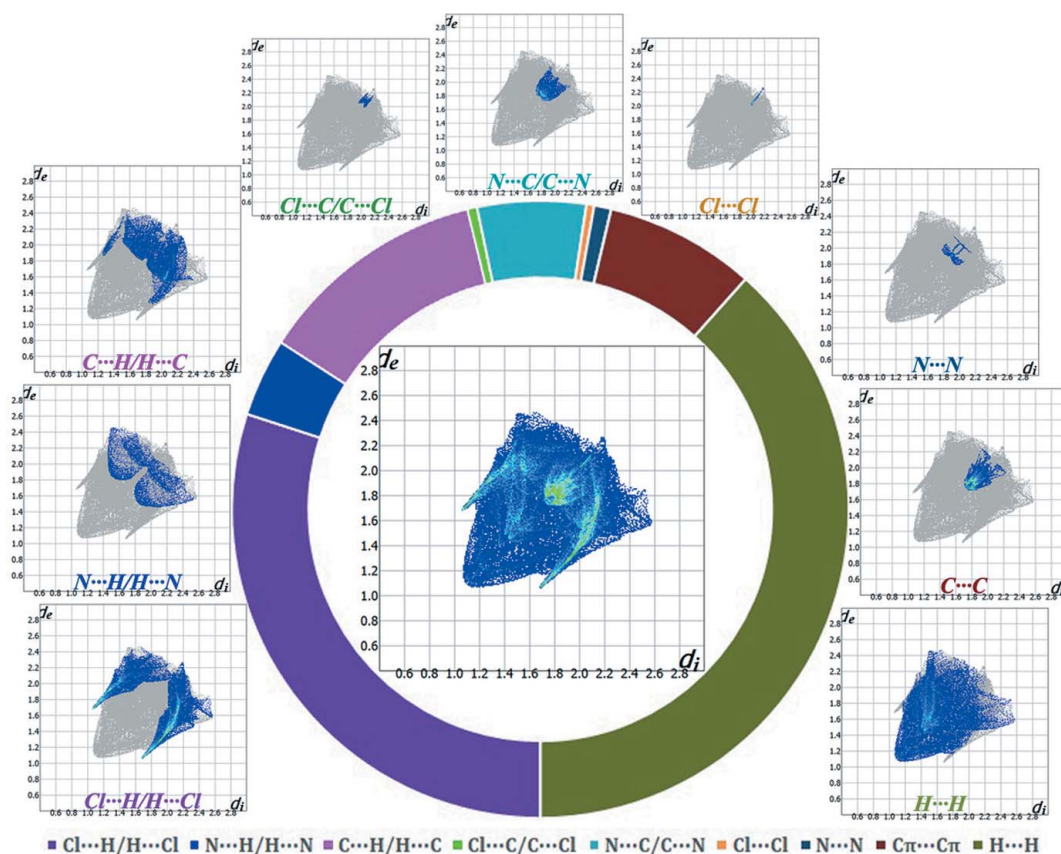
Table 4

Percentage contributions of interatomic contacts to the Hirshfeld surface.

Contact	% contribution	Contact	% contribution
Cl...H/H...Cl	30.0	Cl...Cl	0.4
N...H/H...N	4.1	N...N	0.9
C...H/H...C	12.1	C...C	7.9
Cl...C/C...Cl	0.5	H...H	38.4
N...C/C...N	5.7		

caused by carbon atoms of the π -stacked molecule above it. The presence of π - π stacking is also evident in the flat region toward the bottom of both sides of the molecules and is clearly visible on the curvedness surface (Fig. 4d): the shape of the blue outline on the curvedness surface unambiguously delineates the contacting patches of the molecules. On the d_e surface, this feature appears as a relatively flat green region where the contact distances are similar (Fig. 4b).

The intermolecular interactions present in the structure are also visible on the two-dimensional fingerprint plot (Rohl *et al.*, 2008; Samanta *et al.*, 2014; Seth, 2014a,b,c), which can be decomposed to quantify the individual contributions of each intermolecular interaction involved in the structure (Manna *et al.*, 2014b). These complementary regions are visible in the fingerprint, where one molecule acts as donor ($d_e > d_i$) and the other as an acceptor ($d_i > d_e$). Table 4 contains the percentages


Figure 5

Fingerprint plots: full (middle) and decomposed plots corresponding to all contacts involved in the structure [clockwise: from bottom left to bottom right]. The relative contributions of various intermolecular contacts to the Hirshfeld surface area of the title structure are displayed by the schematic illustration.

of contributions for a variety of contacts in the crystal structure of the title compound.

The C—H···Cl interactions appear as two distinct spikes in the fingerprint plot (Fig. 5) of the title complex, where Cl···H interactions have a larger contribution (18.4%) than their H···Cl counterparts (11.6%). Thus, the sum of Cl···H/H···Cl interactions comprises 30.0% of the total Hirshfeld surface area of the molecule (Table 4). The Cl···H/H···Cl interactions represented by the spikes in the bottom right and left region ($d_e + d_i \simeq 2.77 \text{ \AA}$) indicate that the hydrogen atoms from the ligand moiety are in contact with the metal-coordinated Cl atoms to build the two-dimensional supramolecular framework. The spoon-like tips in the region ($d_e + d_i \simeq 3.37 \text{ \AA}$) of the fingerprint plot (Fig. 5) represent a significant N···H/H···N contribution, covering 4.1% of the total Hirshfeld surface of the molecules. The forceps-like tips in the region ($d_e + d_i \simeq 3.12 \text{ \AA}$) of the fingerprint plot (Fig. 5) represent the C···H/H···C contacts where the C···H counterpart shows a larger contribution (7.6%) than the H···C counterpart (4.5%). Overall, the C···H/H···C interactions account for 12.1% of the total Hirshfeld surface of the molecules (Table 4), and the carbon atoms of the imidazopyridine moiety mainly act as donors in building the molecular assembly. The scattered points in the breakdown of the fingerprint plot show that the π - π stacking interactions comprise 7.9% of the total Hirshfeld surface of the molecule (Table 5) displayed as a region of blue/green color on the

Table 5
Summary of the short interatomic contacts (\AA).

Contact	Distance	Contact	Distance
Cl1···H7 ^v	2.883	C2···H6 ^v	2.992
Cl1···C2 ⁱ	3.613 (2)	C2···C5 ^{iv}	3.535 (3)
Cl1···H2 ⁱ	2.932	C2···H3 ^{viii}	3.021
Cl1···H5 ⁱⁱ	2.893	C4···C4 ^{viii}	3.525 (3)
Cl1···H3 ^{vi}	3.055	C4···H4 ^{viii}	2.834
N1···N1 ⁱ	3.257 (2)	C6···H2 ⁱⁱⁱ	3.050
Cl1···C4 ^{iv}	3.482 (3)	H2···H3 ^{viii}	2.416
Cl1···C5 ^{iv}	3.516 (3)	H4···H4 ^{viii}	2.309
Cl1···C6 ⁱⁱ	3.518 (3)	H6···H2 ⁱⁱⁱ	2.535

Symmetry codes: (i) $-x + \frac{1}{2}, y, -z + \frac{3}{2}$; (ii) $-x, -y, -z + 1$; (iii) $x, y - 1, z$; (iv) $-x + 1, -y, -z + 1$; (v) $x, y + 1, z$; (vi) $x - \frac{1}{2}, -y + 1, z + \frac{1}{2}$; (vii) $-x + 1, -y + 1, -z + 1$; (viii) $-x + \frac{1}{2}, y, -z + \frac{1}{2}$.

diagonal at around $d_e \simeq d_i \simeq 1.743 \text{ \AA}$. Another contribution comes from H···H contacts (38.4%) represented by the scattered points in the fingerprint plots, and spread up only to $d_i = d_e = 1.092 \text{ \AA}$ (Fig. 5).

Finally, the short inter-atomic contacts of the structure (Table 5) of the type Cl···C/ C···Cl, N···C/ C···N, Cl···Cl and N···N are clearly visible as scattered points in the region $d_e + d_i \simeq 4.07 \text{ \AA}$, $d_e + d_i \simeq 3.58 \text{ \AA}$, $d_e + d_i \simeq 4.11 \text{ \AA}$ and $d_e + d_i \simeq 3.82 \text{ \AA}$ of the breakdown fingerprint plots (Fig. 5). They contribute 0.5%, 5.7%, 0.4% and 0.9%, respectively, to the total Hirshfeld area of the title complex (Table 4, see Fig. 6).

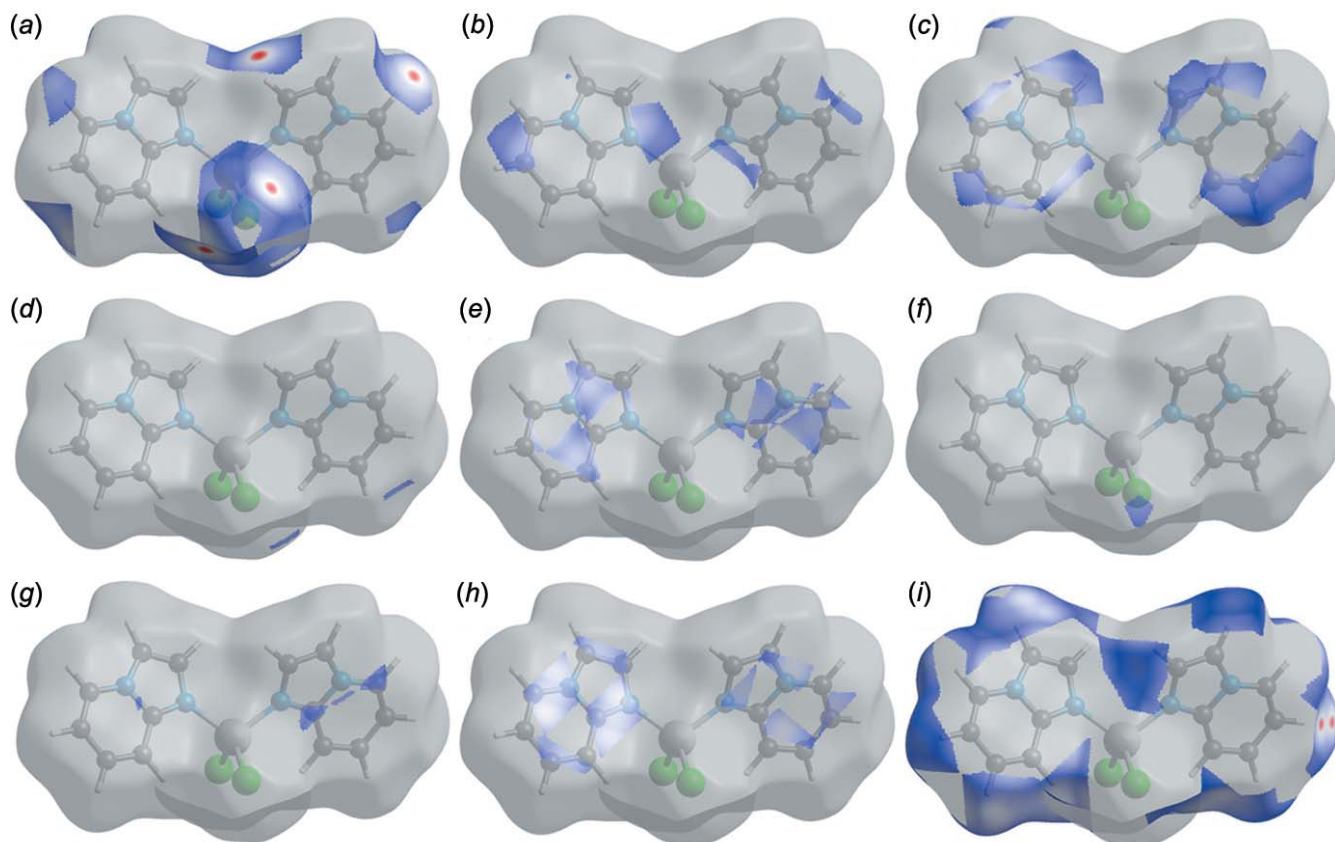


Figure 6
Perspective view of the decomposed d_{norm} surfaces of the title structure corresponding to (a) Cl···H/H···Cl; (b) N···H/H···N; (c) C···H/H···C; (d) Cl···C/C···Cl; (e) N···C/C···N; (f) Cl···Cl; (g) N···N; (h) C···C and (i) H···H contacts.

Table 6
Experimental details.

Crystal data	
Chemical formula	[CoCl ₂ (C ₇ H ₆ N ₂) ₂]
<i>M_r</i>	366.11
Crystal system, space group	Monoclinic, <i>P2₁/n</i>
Temperature (K)	293
<i>a</i> , <i>b</i> , <i>c</i> (Å)	7.712 (2), 6.7898 (18), 14.348 (4)
β (°)	98.533 (5)
<i>V</i> (Å ³)	743.0 (4)
<i>Z</i>	2
Radiation type	Mo <i>K</i> α
μ (mm ⁻¹)	1.51
Crystal size (mm)	0.17 × 0.11 × 0.06
Data collection	
Diffractometer	Bruker <i>SMART</i> APEXII CCD area-detector
Absorption correction	Multi-scan (<i>SADABS</i> ; Bruker, 2007)
<i>T_{min}</i> , <i>T_{max}</i>	0.82, 0.92
No. of measured, independent and observed [<i>I</i> > 2 σ (<i>I</i>)] reflections	6663, 1307, 1241
<i>R_{int}</i>	0.023
($\sin \theta/\lambda$) _{max} (Å ⁻¹)	0.595
Refinement	
<i>R</i> [<i>F</i> ² > 2 σ (<i>F</i> ²)], <i>wR</i> (<i>F</i> ²), <i>S</i>	0.024, 0.064, 1.06
No. of reflections	1307
No. of parameters	96
H-atom treatment	H-atom parameters constrained
$\Delta\rho_{\max}$, $\Delta\rho_{\min}$ (e Å ⁻³)	0.18, -0.32

Computer programs: *APEX2*, *SAINT* and *XPREP* (Bruker, 2007), *SHELXT2014* (Sheldrick, 2015a), *SHELXL2018* (Sheldrick, 2015b), *ORTEP-3 for Windows* (Farrugia, 2012), *DIAMOND* (Brandenburg, 2006), *Mercury* (Macrae *et al.*, 2006) and *PLATON* (Spek, 2009).

The individual intermolecular interactions described above and the quantitative contributions included in Table 4 can be also visualized by the different *d*_{norm} surfaces shown in Fig. 6, confirming that the Hirshfeld surface analysis provides a full understanding of the intermolecular interactions in a facile and immediate way.

5. Database survey

A search in the Cambridge Structural Database (Version 5.38, update May 2017; Groom *et al.*, 2016) for structures of the general formula [ML₂X₂], where *M* is any transition metal, *L* is the ligand imidazo[1,2-*a*]pyridine, and *X* any halogen, yielded no results. However, two related complexes exist, with ruthenium and tin, respectively: (i) dichloro-[2,2'-(pyridine-2,6-diyl)bis(imidazo[1,2-*a*]pyridine)]triphenylphosphineruthenium(II) (GULNEI; Li *et al.*, 2015); (ii) dibromo-bis(imidazo[1,2-*a*]pyridine)dimethyltin (NODREF; Agrawal *et al.*, 2014). In both cases, the presence of the halogen atoms is relevant to the stabilization of the crystal structure. In the case of the ruthenium compound, the complex molecules are linked into discrete supramolecular dimers through pairs of C—H(imidazo)···Cl interactions. On the other hand, the tin complex forms undulating sheets parallel to the (100) plane by means of C—H(pyridine)···Br interactions in which both the Br ions and the ligands of one complex act as acceptor and donor, respectively.

6. Synthesis and crystallization

The title complex was prepared by simple hydrothermal reaction. CoCl₂·6H₂O (2.0 mmol, 0.476 g) was dissolved in water (20 ml) yielding a clear pink solution. A hot water-methanol (1:1) solution (20 ml) of imidazo[1,2-*a*]pyridine (1.0 mmol, 0.118 g) was added dropwise to the above solution under continuous stirring. The solution mixture thus obtained was further heated at 343 K for 2 h and then kept for crystallization at room temperature (303 K). The resulting solution was allowed to evaporate slowly at room temperature for several weeks, yielding testable dark-pink crystals, which were collected by filtration, washed with water and dried in air.

7. Refinement details

Crystal data, data collection and structure refinement details are summarized in Table 6. The hydrogen atoms were located in the difference-Fourier map and refined as riding atoms, with C—H = 0.93 Å and *U*_{iso}(H) = 1.2*U*_{eq}(C).

Funding information

The author is grateful to the Science and Engineering Research Board (SERB) –Department of Science and Technology (DST), Govt. of India for a SERB Overseas Postdoctoral Fellowship (SB/OS/PDF-524/2015–16).

References

- Adib, M., Sheikhi, E. & Rezaei, N. (2011). *Tetrahedron Lett.* **52**, 3191–3194.
- Agrawal, R., Goyal, V., Gupta, R., Pallegogu, R., Kotikalapudi, R., Jones, P. G. & Bansal, R. K. (2014). *Polyhedron*, **70**, 138–143.
- Bagdi, A. K., Santra, S., Monir, K. & Hajra, A. (2015). *Chem. Commun.* **51**, 1555–1575.
- Biftu, T., Feng, D., Fisher, M., Liang, G. B., Qian, X., Scribner, A., Dennis, R., Lee, S., Liberator, P. A., Brown, C., Gurnett, A., Leavitt, P. S., Thompson, D., Mathew, J., Misura, A., Samaras, S., Tamas, T., Sina, J. F., McNulty, K. A., McKnight, C. G., Schmatz, D. M. & Wyratt, M. (2006). *Bioorg. Med. Chem. Lett.* **16**, 2479–2483.
- Brandenburg, K. (2006). *DIAMOND*. Crystal Impact GbR, Bonn, Germany.
- Bravi, G., Cheasty, A. G., Corfield, J. A., Grimes, R. M., Harrison, D., Hartley, C. D., Howes, P. D., Medhurst, K. J., Meeson, M. L., Mordaunt, J. E., *et al.* (2007). World patent WO 2,007,039,146.
- Bruker (2007). *APEX2*, *SAINT*, *XPREP* and *SADABS*. Bruker AXS Inc., Madison, Wisconsin, USA.
- Dymińska, L. (2015). *Bioorg. Med. Chem.* **23**, 6087–6099.
- Enguehard-Gueiffier, C. & Gueiffier, A. (2007). *Mini Rev. Med. Chem.* **7**, 888–899.
- Farrugia, L. J. (2012). *J. Appl. Cryst.* **45**, 849–854.
- Groom, C. R., Bruno, I. J., Lightfoot, M. P. & Ward, S. C. (2016). *Acta Cryst.* **B72**, 171–179.
- Gudmundsson, K. S. & Boggs, S. D. (2007). World patent WO 2,007,027,999.
- Gudmundsson, K. S. & Johns, B. A. (2007). *Bioorg. Med. Chem. Lett.* **17**, 2735–2739.
- Gunja, N. (2013). *J. Med. Toxicol.* **9**, 163–171.
- Harrison, T. S. & Keating, G. M. (2005). *CNS Drugs*, **19**, 709–716.
- Ismail, M. A., Arafa, R. K., Wenzler, T., Brun, R., Tanius, F. A., Wilson, W. D. & Boykin, D. W. (2008). *Bioorg. Med. Chem.* **16**, 683–691.

- Kaminski, J. J. & Doweiko, A. M. (1997). *J. Med. Chem.* **40**, 427–436.
- Ke, C.-H., Kuo, B.-C., Nandi, D. & Lee, H. M. (2013). *Organometallics*, **32**, 4775–4784.
- Li, K., Niu, J.-L., Yang, M.-Z., Li, Z., Wu, L.-Y., Hao, X.-Q. & Song, M.-P. (2015). *Organometallics*, **34**, 1170–1176.
- Macrae, C. F., Edgington, P. R., McCabe, P., Pidcock, E., Shields, G. P., Taylor, R., Towler, M. & van de Streek, J. (2006). *J. Appl. Cryst.* **39**, 453–457.
- Manna, P., Ray Choudhury, S., Mitra, M., Kumar Seth, S., Helliwell, M., Bauzá, A., Frontera, A. & Mukhopadhyay, S. (2014b). *J. Solid State Chem.* **220**, 149–156.
- Manna, P., Seth, S. K., Das, A., Hemming, J., Prendergast, R., Helliwell, M., Choudhury, S. R., Frontera, A. & Mukhopadhyay, S. (2012). *Inorg. Chem.* **51**, 3557–3571.
- Manna, P., Seth, S. K., Mitra, M., Choudhury, S. R., Bauzá, A., Frontera, A. & Mukhopadhyay, S. (2014a). *Cryst. Growth Des.* **14**, 5812–5821.
- Manna, P., Seth, S. K., Mitra, M., Das, A., Singh, N. J., Choudhury, S. R., Kar, T. & Mukhopadhyay, S. (2013). *CrystEngComm*, **15**, 7879–7886.
- McKinnon, J. J., Jayatilaka, D. & Spackman, M. A. (2007). *Chem. Commun.* pp. 3814–3816.
- McKinnon, J. J., Mitchell, A. S. & Spackman, M. A. (1998). *Chem. Eur. J.* **4**, 2136–2141.
- Mitra, M., Manna, P., Bauzá, A., Ballester, P., Seth, S. K., Ray Choudhury, S., Frontera, A. & Mukhopadhyay, S. (2014). *J. Phys. Chem. B*, **118**, 14713–14726.
- Mitra, M., Seth, S. K., Choudhury, S. R., Manna, P., Das, A., Helliwell, M., Bauzá, A., Frontera, A. & Mukhopadhyay, S. (2013). *Eur. J. Inorg. Chem.* pp. 4679–4685.
- Prostota, Y., Kachkovsky, O. D., Reis, L. V. & Santos, P. F. (2013). *Dyes Pigments*, **96**, 554–562.
- Puerstinger, G., Paeshuysse, J., De Clercq, E. & Neyts, J. (2007). *Bioorg. Med. Chem. Lett.* **17**, 390–393.
- Rival, Y., Grassy, G. & Michel, G. (1992). *Chem. Pharm. Bull.* **40**, 1170–1176.
- Rival, Y., Grassy, G., Taudou, A. & Ecalle, R. (1991). *Eur. J. Med. Chem.* **26**, 13–18.
- Rohl, A. L., Moret, M., Kaminsky, W., Claborn, K., McKinnon, J. J. & Kahr, B. (2008). *Cryst. Growth Des.* **8**, 4517–4525.
- Rupert, K. C., Henry, J. R., Dodd, J. H., Wadsworth, S. A., Cavender, D. E., Olini, G. C., Fahmy, B. & Siekierka, J. J. (2003). *Bioorg. Med. Chem. Lett.* **13**, 347–350.
- Samanta, T., Dey, L., Dinda, J., Chattopadhyay, S. K. & Seth, S. K. (2014). *J. Mol. Struct.* **1068**, 58–70.
- Seth, S. K. (2013). *CrystEngComm*, **15**, 1772–1781.
- Seth, S. K. (2014a). *J. Mol. Struct.* **1064**, 70–75.
- Seth, S. K. (2014b). *J. Mol. Struct.* **1070**, 65–74.
- Seth, S. K. (2014c). *Inorg. Chem. Commun.* **43**, 60–63.
- Seth, S. K., Manna, P., Singh, N. J., Mitra, M., Jana, A. D., Das, A., Choudhury, S. R., Kar, T., Mukhopadhyay, S. & Kim, K. S. (2013). *CrystEngComm*, **15**, 1285–1288.
- Seth, S. K., Saha, I., Estarellas, C., Frontera, A., Kar, T. & Mukhopadhyay, S. (2011b). *Cryst. Growth Des.* **11**, 3250–3265.
- Seth, S. K., Sarkar, D., Jana, A. D. & Kar, T. (2011d). *Cryst. Growth Des.* **11**, 4837–4849.
- Seth, S. K., Sarkar, D. & Kar, T. (2011a). *CrystEngComm*, **13**, 4528–4535.
- Seth, S. K., Sarkar, D., Roy, A. & Kar, T. (2011c). *CrystEngComm*, **13**, 6728–6741.
- Sheldrick, G. M. (2015a). *Acta Cryst.* **A71**, 3–8.
- Sheldrick, G. M. (2015b). *Acta Cryst.* **C71**, 3–8.
- Spackman, M. A. & Byrom, P. G. (1997). *Chem. Phys. Lett.* **267**, 215–220.
- Spackman, M. A. & McKinnon, J. J. (2002). *CrystEngComm*, **4**, 378–392.
- Spek, A. L. (2009). *Acta Cryst.* **D65**, 148–155.
- Véron, J. B., Enguehard-Gueiffier, C., Snoeck, R., Andrei, G., De Clercq, E. & Gueiffier, A. (2007). *Bioorg. Med. Chem.* **15**, 7209–7219.
- Wolff, S. K., Grimwood, D. J., McKinnon, J. J., Jayatilaka, D. & Spackman, M. A. (2012). *CrystalExplorer 3.1*. The University of Western Australia.

supporting information

Acta Cryst. (2018). E74, 600-606 [https://doi.org/10.1107/S2056989018003857]

Structural characterization and Hirshfeld surface analysis of a Co^{II} complex with imidazo[1,2-a]pyridine

Saikat Kumar Seth

Computing details

Data collection: *APEX2* (Bruker, 2007); cell refinement: *APEX2* (Bruker, 2007) and *SAINT* (Bruker, 2007); data reduction: *SAINT* (Bruker, 2007) and *XPREP* (Bruker, 2007); program(s) used to solve structure: *SHELXT2014* (Sheldrick, 2015a); program(s) used to refine structure: *SHELXL2018* (Sheldrick, 2015b); molecular graphics: *ORTEP-3 for Windows* (Farrugia, 2012), *DIAMOND* (Brandenburg, 2006) and *Mercury* (Macrae *et al.*, 2006); software used to prepare material for publication: *PLATON* (Spek, 2009).

Dichloridobis(imidazo[1,2-a]pyridine- κ N¹)cobalt(II)

Crystal data

[CoCl₂(C₇H₆N₂)₂]

$M_r = 366.11$

Monoclinic, *P2₁/n*

$a = 7.712$ (2) Å

$b = 6.7898$ (18) Å

$c = 14.348$ (4) Å

$\beta = 98.533$ (5)°

$V = 743.0$ (4) Å³

$Z = 2$

$F(000) = 370$

$D_x = 1.636$ Mg m⁻³

Mo $K\alpha$ radiation, $\lambda = 0.71073$ Å

Cell parameters from 647 reflections

$\theta = 1.5$ – 25.0 °

$\mu = 1.51$ mm⁻¹

$T = 293$ K

Block, pink

$0.17 \times 0.11 \times 0.06$ mm

Data collection

Bruker SMART APEXII CCD area-detector diffractometer

Radiation source: fine-focus sealed tube

Graphite monochromator

ω and φ scans

Absorption correction: multi-scan (SADABS; Bruker, 2007)

$T_{\min} = 0.82$, $T_{\max} = 0.92$

6663 measured reflections

1307 independent reflections

1241 reflections with $I > 2\sigma(I)$

$R_{\text{int}} = 0.023$

$\theta_{\max} = 25.0$ °, $\theta_{\min} = 2.8$ °

$h = -8 \rightarrow 9$

$k = -8 \rightarrow 8$

$l = -17 \rightarrow 17$

Refinement

Refinement on F^2

Least-squares matrix: full

$R[F^2 > 2\sigma(F^2)] = 0.024$

$wR(F^2) = 0.064$

$S = 1.06$

1307 reflections

96 parameters

0 restraints

Primary atom site location: structure-invariant direct methods

Secondary atom site location: difference Fourier map

Hydrogen site location: inferred from neighbouring sites

H-atom parameters constrained

$$w = 1/[\sigma^2(F_o^2) + (0.0355P)^2 + 0.2499P]$$

where $P = (F_o^2 + 2F_c^2)/3$
 $(\Delta/\sigma)_{\max} < 0.001$

$$\Delta\rho_{\max} = 0.18 \text{ e } \text{\AA}^{-3}$$

$$\Delta\rho_{\min} = -0.31 \text{ e } \text{\AA}^{-3}$$

Special details

Geometry. All esds (except the esd in the dihedral angle between two l.s. planes) are estimated using the full covariance matrix. The cell esds are taken into account individually in the estimation of esds in distances, angles and torsion angles; correlations between esds in cell parameters are only used when they are defined by crystal symmetry. An approximate (isotropic) treatment of cell esds is used for estimating esds involving l.s. planes.

Refinement. Refinement of F^2 against ALL reflections. The weighted R-factor wR and goodness of fit S are based on F^2 , conventional R-factors R are based on F, with F set to zero for negative F^2 . The threshold expression of $F^2 > 2\sigma(F^2)$ is used only for calculating R-factors(gt) etc. and is not relevant to the choice of reflections for refinement. R-factors based on F^2 are statistically about twice as large as those based on F, and R-factors based on ALL data will be even larger.

Fractional atomic coordinates and isotropic or equivalent isotropic displacement parameters (\AA^2)

	x	y	z	$U_{\text{iso}}^*/U_{\text{eq}}$
Co1	0.250000	0.21247 (5)	0.750000	0.03788 (13)
Cl1	0.00699 (6)	0.40150 (8)	0.73557 (4)	0.05261 (16)
N1	0.2270 (2)	0.0373 (2)	0.63532 (10)	0.0410 (3)
N2	0.2373 (2)	-0.0539 (2)	0.48712 (11)	0.0452 (4)
C2	0.3250 (3)	0.2781 (3)	0.52292 (15)	0.0513 (5)
H2	0.341071	0.383348	0.564797	0.062*
C1	0.2664 (2)	0.0958 (3)	0.55145 (12)	0.0386 (4)
C6	0.1741 (3)	-0.2106 (3)	0.53192 (17)	0.0554 (5)
H6	0.141218	-0.332623	0.505604	0.066*
C5	0.2770 (3)	-0.0324 (4)	0.39615 (14)	0.0635 (6)
H5	0.261300	-0.136802	0.353786	0.076*
C7	0.1689 (3)	-0.1537 (3)	0.62194 (16)	0.0503 (5)
H7	0.131285	-0.232355	0.668094	0.060*
C3	0.3582 (3)	0.2988 (4)	0.43289 (15)	0.0629 (6)
H3	0.394972	0.419967	0.412794	0.075*
C4	0.3379 (3)	0.1406 (5)	0.37060 (15)	0.0677 (7)
H4	0.367003	0.155512	0.310375	0.081*

Atomic displacement parameters (\AA^2)

	U^{11}	U^{22}	U^{33}	U^{12}	U^{13}	U^{23}
Co1	0.0447 (2)	0.0343 (2)	0.0365 (2)	0.000	0.01225 (14)	0.000
Cl1	0.0507 (3)	0.0496 (3)	0.0578 (3)	0.0098 (2)	0.0093 (2)	0.0003 (2)
N1	0.0469 (8)	0.0342 (8)	0.0436 (8)	-0.0029 (6)	0.0121 (7)	-0.0024 (6)
N2	0.0415 (8)	0.0476 (9)	0.0451 (9)	0.0027 (7)	0.0022 (7)	-0.0107 (7)
C2	0.0594 (12)	0.0493 (11)	0.0442 (11)	-0.0098 (9)	0.0045 (9)	0.0033 (9)
C1	0.0383 (9)	0.0406 (10)	0.0367 (9)	0.0018 (7)	0.0049 (7)	-0.0037 (7)
C6	0.0561 (12)	0.0403 (11)	0.0677 (14)	-0.0017 (9)	0.0023 (10)	-0.0165 (9)
C5	0.0534 (12)	0.0963 (18)	0.0387 (11)	0.0085 (13)	-0.0003 (9)	-0.0252 (12)
C7	0.0520 (11)	0.0353 (9)	0.0644 (12)	-0.0050 (9)	0.0109 (9)	0.0038 (9)
C3	0.0607 (13)	0.0808 (16)	0.0454 (11)	-0.0161 (12)	0.0019 (10)	0.0154 (11)
C4	0.0540 (13)	0.111 (2)	0.0381 (11)	-0.0105 (14)	0.0054 (9)	0.0056 (13)

Geometric parameters (Å, °)

Co1—N1	2.0168 (4)	C2—C1	1.400 (3)
Co1—N1 ⁱ	2.0169 (15)	C2—H2	0.9300
Co1—C11	2.2556 (5)	C6—C7	1.355 (3)
Co1—C11 ⁱ	2.2556 (7)	C6—H6	0.9300
N1—C1	1.344 (2)	C5—C4	1.337 (4)
N1—C7	1.376 (2)	C5—H5	0.9300
N2—C1	1.369 (2)	C7—H7	0.9300
N2—C6	1.370 (3)	C3—C4	1.391 (4)
N2—C5	1.392 (3)	C3—H3	0.9300
C2—C3	1.361 (3)	C4—H4	0.9300
N1—Co1—N1 ⁱ	107.70 (5)	N2—C1—C2	119.15 (17)
N1—Co1—C11	106.83 (1)	C7—C6—N2	106.79 (17)
N1 ⁱ —Co1—C11	112.44 (5)	C7—C6—H6	126.6
N1—Co1—C11 ⁱ	112.44 (5)	N2—C6—H6	126.6
N1 ⁱ —Co1—C11 ⁱ	106.83 (5)	C4—C5—N2	119.0 (2)
C11—Co1—C11 ⁱ	110.64 (4)	C4—C5—H5	120.5
C1—N1—C7	105.44 (16)	N2—C5—H5	120.5
C1—N1—Co1	123.48 (12)	C6—C7—N1	110.28 (19)
C7—N1—Co1	131.06 (14)	C6—C7—H7	124.9
C1—N2—C6	107.13 (16)	N1—C7—H7	124.9
C1—N2—C5	121.17 (19)	C2—C3—C4	120.7 (2)
C6—N2—C5	131.65 (19)	C2—C3—H3	119.6
C3—C2—C1	118.9 (2)	C4—C3—H3	119.6
C3—C2—H2	120.5	C5—C4—C3	120.9 (2)
C1—C2—H2	120.5	C5—C4—H4	119.6
N1—C1—N2	110.35 (16)	C3—C4—H4	119.6
N1—C1—C2	130.48 (17)		
N1 ⁱ —Co1—N1—C1	-157.31 (17)	C5—N2—C1—C2	4.7 (3)
C11 ⁱ —Co1—N1—C1	-39.88 (15)	C3—C2—C1—N1	179.1 (2)
C11—Co1—N1—C1	81.68 (14)	C3—C2—C1—N2	-2.6 (3)
N1 ⁱ —Co1—N1—C7	24.35 (15)	C1—N2—C6—C7	-0.9 (2)
C11 ⁱ —Co1—N1—C7	141.78 (16)	C5—N2—C6—C7	176.8 (2)
C11—Co1—N1—C7	-96.66 (17)	C1—N2—C5—C4	-2.7 (3)
C7—N1—C1—N2	-1.1 (2)	C6—N2—C5—C4	180.0 (2)
Co1—N1—C1—N2	-179.77 (11)	N2—C6—C7—N1	0.2 (2)
C7—N1—C1—C2	177.4 (2)	C1—N1—C7—C6	0.5 (2)
Co1—N1—C1—C2	-1.3 (3)	Co1—N1—C7—C6	179.08 (14)
C6—N2—C1—N1	1.2 (2)	C1—C2—C3—C4	-1.3 (3)
C5—N2—C1—N1	-176.69 (16)	N2—C5—C4—C3	-1.3 (3)
C6—N2—C1—C2	-177.42 (18)	C2—C3—C4—C5	3.4 (4)

Symmetry code: (i) $-x+1/2, y, -z+3/2$.

Hydrogen-bond geometry (Å, °)

<i>D</i> —H \cdots <i>A</i>	<i>D</i> —H	H \cdots <i>A</i>	<i>D</i> \cdots <i>A</i>	<i>D</i> —H \cdots <i>A</i>
C5—H5 \cdots Cl1 ⁱⁱ	0.93	2.89	3.663 (1)	141
C7—H7 \cdots Cl1 ⁱⁱⁱ	0.93	2.88	3.734 (1)	153

Symmetry codes: (ii) $-x, -y, -z+1$; (iii) $x, y-1, z$.